J Fluoresc (2008) 18:239–245
DOI 10.1007/s10895-007-0195-z

ORIGINAL PAPER

Synthesis, Characterization and Photophysical Properties of Eu^{3+} Doped in $BaMoO_4$

Ieda L. V. Rosa · Ana Paula A. Marques · Marcos T. S. Tanaka · Dulce M. A. Melo · Edson R. Leite · Elson Longo · José Arana Varela

Received: 4 January 2007 / Accepted: 10 April 2007 / Published online: 20 December 2007

Abstract In this work $Ba_{0.99}Eu_{0.01}MoO_4$ (BEMO) powders were prepared by the first time by the Complex Polymerization Method. The structural and optical properties of the BEMO powders were characterized by Fourier Transform Infra-Red (FTIR), X-ray Diffraction (XRD), Raman Spectra, High-Resolution Scanning Electron Microscopy (HR-SEM) and Photoluminescent Measurements. XRD show a crystalline scheelite-type phase after the heat treatment at temperatures greater than 400 °C. The ionic radius of Eu^{3+} (0.109 nm) is lower than the Ba^{2+} (0.149 nm) one. This difference is responsible for the decrease in the lattice parameters of the BEMO compared to the pure $BaMoO_4$ matrix. This little difference in the lattice parameters show that Eu^{3+} is expected to occupy the Ba^{2+} site at different temperatures, stayed the tetragonal (S_4) symmetry characteristic of scheelite-type crystalline structures of $BaMoO_4$. The emission spectra of the samples, when excited at 394 nm, presented the $^5D_1 \rightarrow {}^7F_{0,\ 1\ \text{and}\ 2}$ and $^5D_0 \rightarrow {}^7F_{0,\ 1,\ 2,\ 3\ \text{and}\ 4}$ Eu^{3+} transitions at 523, 533, 554, 578, 589, 614, 652 and 699 nm, respectively. The emission spectra of the powders heat-treated at 800 and 900 °C showed a marked increase in its intensities compared to the materials heat-treated from 400 to 700 °C. The decay times for the sample were evaluated and all of them presented the average value of 0.61 ms. Eu^{3+} luminescence decay time follows one exponential curve indicating the presence of only one type of Eu^{3+} symmetry site.

Keywords Europium · Molybdate · Complex Polymerization Method · Photoluminescence

I. L. V. Rosa (✉) · M. T. S. Tanaka · E. R. Leite
LIEC-CMDMC, DQ, UFSCar, Via Washinton Luiz, km 235, CEP 13565-905, São Carlos, Sao Paulo, Brazil
e-mail: ilvrosa@power.ufscar.br

A. P. A. Marques · D. M. A. Melo
Laboratório de Análise Térmica e Materiais, DQ, UFRN, 59072-970, Natal, Rio Grande do Norte, Brazil

E. Longo
LIEC-CMDMC, IQ, UNESP, Rua Francisco Degni s/n, CEP 14800-900, Araraquara, Sao Paulo, Brazil

J. A. Varela
CMDMC, LIEC, Instituto de Química, Universidade Estadual Paulista, 14801-907, Araraquara, Sao Paulo, Brazil

Introduction

Numerous investigations on the luminescent properties of scheelite-type crystalline structures, such as $BaMoO_4$ (BMO), have been carried out. This kind of compounds have attracted great attention due to their applications as scintillating materials in electro-optical like solid-state lasers and optical fibres [1].

One of the main problems concerning the preparation of the molybdates powders by conventional solid-state reaction method is the synthesis of powders with large grain size and irregular morphology [2]. Such drawbacks could be minimized using the Complex Polymerization Method (CPM) since this synthesis occurs at a low temperature and the immobilization of the metal complexes in such rigid organic polymeric networks can reduce the metal segregation, thus ensuring the compositional homogeneity at the molecular scale. The cation distribution throughout the entire gel system is of fundamental importance for the synthesis of multicomponent oxides since the chemical homogeneity often determines the compositional homogeneity of the material [3, 4]. The studies about luminescent properties of BMO doped with rare earth are still scarce

nowadays. However, molybdates (MoO_4^{2-}) can be opted for host material once in the MoO_4^{2-} the central Mo metal ion is coordinated by four O^{2-} ions in a relatively stable tetrahedral symmetry (Td) belong to the tetragonal crystal structure of space group $I4_1/a$. So, trivalent europium ion (Eu^{3+}) activated calcium molybdates ($CaMoO_4$) phosphor has been developed by solid-state reaction in air, and its luminescent properties were recently investigated [5]. In this structure, the Eu^{3+} impurity is occupying the host divalent cation sites with tetragonal symmetry (S_4) [6, 7].

Eu^{3+} ions have attracted significant attention due to their potential application as phosphors, electroluminescent devices, optical amplifiers or lasers when it is used as doping in a variety of several materials [8–10]. Eu^{3+} is the most studied by luminescence spectroscopy among the rare earth ions, owing to the simplicity of its spectra and because of its application as red phosphor in TV screen [11]. The luminescence of the Eu^{3+} presents emission lines extending from visible to near infrared with a relatively simple energy level structure. Especially the $^5D_0 \rightarrow {}^7F_J$ (J=0,1,2,…6) manifold enables one to ascertain the microscopic symmetry around the site, making the Eu^{3+} an ideal experimental probe of the crystalline environment [12]. The Eu^{3+} ion excited by 394 nm light ($^5L_6$ level) normally decays in inorganic systems to the ^5D levels, mainly to the $^5D_0$, from which the ground state is reached with emission of radiation to the levels of the fundamental term ^7F_J (J=0,1,2,… 6) [13]. The ($2J$+1) degeneracy of the free ion may be broken by the crystal field at its location. The levels with J=0 are not degenerated, and the $^5D_0 \rightarrow {}^7F_0$ transition shows no more than one band, $^5D_0 \rightarrow {}^7F_1$ three bands and $^5D_0 \rightarrow {}^7F_2$ five bands, if the Eu^{3+} sites have a only one symmetry. Changes in the environment can cause only a slight change in the position of the electronic transition lines of the rare earth ions; however, very different values in its luminescence lifetime have been observed [14, 15].

In this work $Ba_{0.99}Eu_{0.01}MoO_4$ powders (BEMO) were prepared for the first time by the Complex Polymerization Method (CPM) and characterized by Fourier Transformed Infra-Red (FTIR), X-ray diffraction (XRD), Raman spectra, high-resolution scanning electron microscopy (HR-SEM) and photoluminescent measurements.

Experimental

Materials

Molybdenum trioxide MoO_3 (Synth 85%), $BaCO_3$ (Mallinckrodt 99%), europium (III) oxide (Aldrich, USA, purity > 99.90%), citric acid ($H_3C_6H_5O_7$) (Mallinckrodt 99%) and ethylene glycol ($HOCH_2CH_2OH$) (J. T. Baker 99%). All of the chemicals were used without further purification.

Synthesis

BEMO powders were prepared by the CPM, which flow chart is outlined at Fig. 1. Molybdenum citrate was formed by the dissolution of MoO_3, molybdenum trioxide, in an aqueous solution of citric acid under constant stirring at 60–80 °C until complete homogenization of the solution. Barium carbonate and europium chloride were then added to the molybdenum citrate solution. The complex was stirred for several hours at 60–80 °C to produce a clear and homogeneous solution. After that, ethylene glycol was added to promote the polyesterification. The viscosity of the solution increases with continued heating at 80–90 °C, and the reactional mixture presented no phase separation. The molar ratio between barium and europium was 99:1, between these cations and molybdenum was 1:1, and the ratio between citric acid and the sum of metals was 6:1. The citric acid/ethylene glycol mass ratio was set at 60:40. After partial evaporation of the water, the resin was heat treated at 300 °C for 2 h in a static atmosphere, leading to the partial decomposition of the polymeric gel, forming an expanded resin, constituted of partially pyrolyzed material. The product was removed from the becker and deagglomerated. The powders were annealed in the temperature range of 400 to 900 °C for 2 h in a static atmosphere and with a heating rate of 5 °C/min.

Characterizations

BEMO powders were characterized by X-ray diffraction (XRD) in a Rigaku Dmax2500PC diffractometer, using a Cu Kα radiation in order to determine the structural evaluation and the unit cell volume of the powders. The average crystallite diameter (Dcrys) of the heat-treated

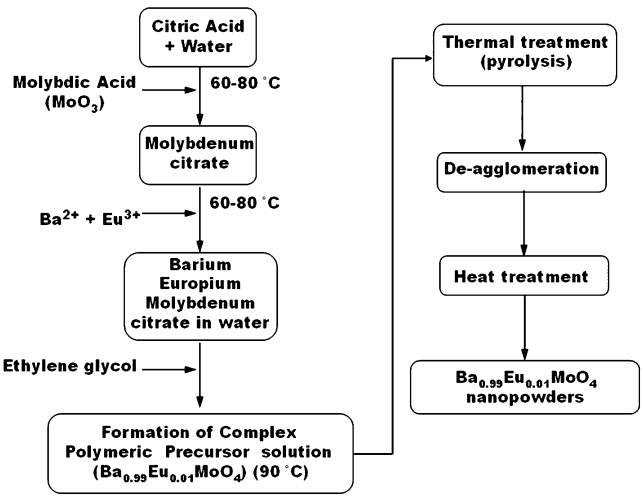

Fig. 1 Flow chart representing the procedure used for the synthesis of BEMO powders

powders was determined by XRD, using the (112) diffraction peak of the $BaMoO_4$ phase (2θ at around 26.5°) according to the Scherrer equation, as described by Suryanarayana [16],

$$B = k \times \lambda / (D_{crys} \times \cos\theta), \quad (1)$$

where B is the full width at half maximum (FWHM), θ the Bragg angle, k is a constant and λ is the wavelength of the Cu Kα radiation.

The BEMO Fourier Transformed Infra-Red (FTIR) transmittance spectra were recorded at 380–3,000 cm^{-1} frequency range as pressed discs (1% by weight in CsI) at room temperature, using an Equinox/55 (Bruker) spectrometer. The BEMO and BMO Raman spectroscopy data were obtained at room temperature using a RFS/100/S Bruker FT-Raman equipment with spectral resolution of 4 cm^{-1} attached to a Nd:YAG laser, promoting an excitation light of 1,064 nm in the frequency range of 100–1,000 cm^{-1}. The photoluminescence data of the BEMO powders were obtained under a 450 W xenon lamp in a Jobin Yvon-Fluorolog spectrofluorometer at room temperature. Luminescence lifetime measurements were carried out as well using a 1934D model spectrophosphorometer coupled to the spectrofluorometer.

Results and discussion

The work presented by Hu et al. [5] deals with the synthesis of $CaMoO_4:Eu^{3+}$ through the solid-state reaction in air. In this present work the method utilized to the synthesis of $Ba_{0.99}Eu_{0.01}MoO_4$ was the Complex Polymerization Method (CPM) that shown to be efficient for the synthesis of BEMO and BMO powders presenting characteristics like small sized grants and high morphological homogeneity, which are difficult to observed using the solid-state reaction method. Figure 2 shows the XRD patterns of the BEMO samples heat treated at different temperatures, as well as BMO XRD patterns for comparison. This figure shows a crystalline scheelite-type phase for all samples heat treated at 400 °C and higher temperatures. All diffraction peaks were indexed according to JCPDS data base n° 29-0193. From the peak positions displayed in Fig. 2, the lattice parameters were calculated using the least square refinement from the REDE93 program. Table 1 presents the crystallite sizes and lattice constants of tetragonal structure of BEMO powders prepared by the CPM and heat treated at different temperatures. The calculated mean crystallite sizes showed the tendency to increase when the heat treatment temperature increases. The lattice constants for the BEMO crystalline powder heat treated at 900 °C were evaluated by XRD data, using the (112) diffraction peak of the

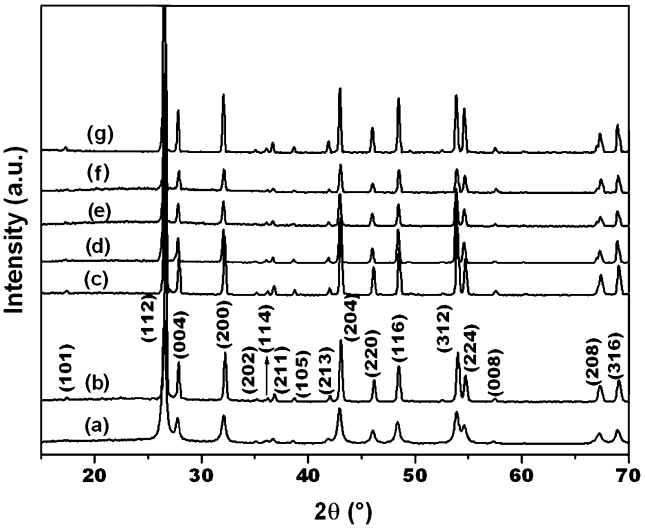

Fig. 2 X-ray diffraction patterns of BEMO powders heat-treated at (**a**) 400 °C, (**b**) 500 °C, (**c**) 600 °C, (**d**) 700 °C, (**e**) 800 °C and (**f**) 900 °C. BMO XRD patterns are presented in (**g**)

BEMO phase (2θ at around 26.5°) and were determined as a=5.5758 Å, c=12.7942 Å, while the pure $BaMoO_4$ matrix presents a=5.5802 Å and c=12.821 Å. These results show evidence of the stabilization of an uncoupled charge disproportionation Ba^{2+} and Eu^{3+}:

$$Eu_2Cl_3 \xrightarrow{BaMoO_4} 2Eu^{\bullet}_{Ba} + V^{II}_{Ba} + 3/2\ Cl_2 \quad (2)$$

where: V^{II}_{Ba} is barium vacancy and $Eu^{\bullet}_{Ba}$ charge of europium ion, and the barium vacancy in Eq. 2 would compensate the charge of two europium ion. This is possible because the europium ion has a charge greater than barium charge causing more defects (vacancies) in the material.

The mean charge modulation between Eu^{3+} and Ba^{2+} sites is about an electron. The values of crystallite sizes (calculated using the (112), 100% diffraction peak) for the BEMO powders are near to 46 nm, which is a similar value reported for BMO prepared by the same method [4]. Since

Table 1 Crystallite sizes and lattice constants of the tetragonal structure of BEMO powders prepared by the CPM method and heat treated at different temperatures

Sample BEMO	Crystallite sizes (nm)	Lattice constants (Å)	
		a	*c*
400 °C	27 (±1.3)	5.575(2)	12.826(6)
500 °C	41 (±2.1)	5.564(1)	12.820(5)
600 °C	44 (±2.2)	5.572(1)	12.802(4)
700 °C	48 (±2.4)	5.581(0.5)	12.818(2)
800 °C	47 (±2.4)	5.579(0.3)	12.816(1)
900 °C	46 (±2.3)	5.576(0.5)	12.794(2)

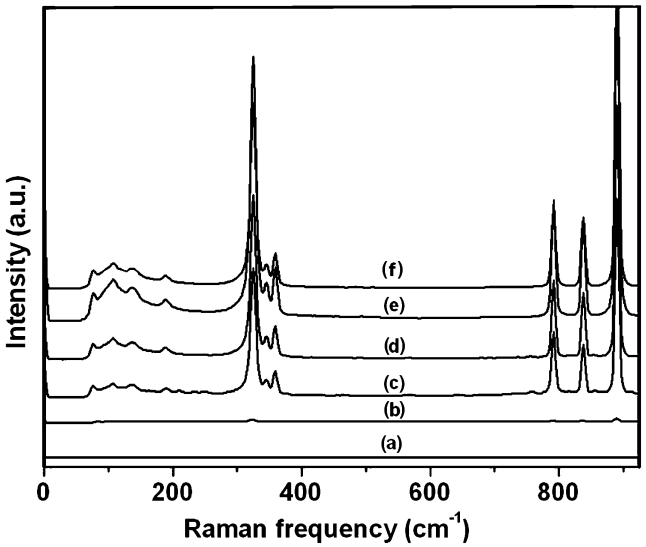

Fig. 3 Spontaneous Raman spectra of BEMO powders heat-treated at 400 °C (**a**), 500 °C (**b**), 600 °C (**c**), 700 °C (**d**), 800 °C (**e**) and 900 °C (**f**)

the Eu^{3+} ratio is almost the same for the substituted Ba^{2+}, it is expected here that Eu^{3+} presents the same Ba^{2+} symmetry ascribed to S_4.

Figure 3 presents the Raman spectra of the Raman-active vibration modes of the BEMO powders heat treated at 400 (a), 500 (b), 600 (c), 700 (d), 800 (e) and 900 °C (f). The assignments of the Raman-active vibration modes of these materials are detailed in Table 2. The primitive cell of $BaMoO_4$ includes two formula units according to Basiev et al. [17]. The $[MoO_4]^{2-}$ ionic group, with strong covalent Mo–O bonds, is peculiar to the $BaMoO_4$ scheelite structure. Due to weak coupling between the $[MoO_4]^{2-}$ ionic group and the Ba^{2+} cations, the vibrational modes observed in the spontaneous Raman spectra of $BaMoO_4$ scheelite crystals can be divided into two groups of internal and external modes. The internal vibrational modes correspond to the vibrations within the $[MoO_4]^{2-}$ group, with a rigid mass center. The external or lattice phonons correspond to the motion of the Ba^{2+} cations and the rigid molecular unit. The $[MoO_4]^{2-}$ tetrahedral have a Td-symmetry in the free space.

The scheelite primitive cell presents twenty six different vibrational modes: $\Gamma_{Td}=3A_g+5A_u+5B_g+3B_u+5E_g+5E_u$, but only the A_g, B_g and E_g ones are Raman-active, while the odd modes $4A_u$ and $4E_u$ can only be registered in the infrared spectra. The tree B_u vibrations are silent modes whereas one A_u and one E_u modes are acoustic vibrations [17]. The Raman spectra presented at Fig. 3c–f showed the well-resolved sharp peaks for the BEMO powders heat treated at 600–900 °C, indicating that the synthesized powders were highly crystallized. The Raman spectra of BEMO powders annealed at 400 and 500 °C does not present such well-resolved sharp peaks (Fig. 3a–b). Its crystallization was however observed by XRD (Fig. 2a–b). This difference was understood by the fact that the X-ray probes the overall long-range order, whereas Raman scattering probes the short-range structural order.

Figure 4 presents a HR-SEM micrograph of BEMO powders heat treated at 700 °C (a) and 900 °C (b) with a heating rate of 5 °C/min. In this figure was observed that the BEMO sample heat treated at 700 °C (Fig. 4a) presents an agglomerate of individual particles, which sizes are less than 100 nm. The BEMO powders heat treated at 900 °C (Fig. 4b) showed small particles of BEMO with dimensions of around 100 nm and that probable will be embodied to form one bigger particle. In this case occur the growth of the grains, favoring the sintherizing process and consequently it is observed a bigger crystallite size than that observed for the BEMO sample heat treated at 700 °C.

Table 2 Raman mode frequencies for the BEMO powders heat treated at different temperatures

Lattice mode symmetry C^6_{4h}	BEMO[a,b]		BMO[a]	BMO[c,2]	Assignments
	500 °C	600–900 °C	500–700 °C	1,100–1,200 °C	
A_g	889	890	891	892	ν_1 (A_1)
B_g	838	838	838	837	ν_3 (F_2)
E_g	789	791	791	791	
E_g	359	359	359	358	ν_4 (F_2)
B_g		346	346	345	
B_g		325	326	324	ν_2 (E)
A_g	325	325	325	324	
E_g		190	190	188	$\nu_{f.r.}$ (F_1) free rotation
B_g		138	141	137	$\nu_{ext.}$-external modes MoO_4^{2-} and Ba^{2+} motions
E_g		108	107	110	
B_g		78	78	76	
E_g			76	74	

[a] CPM method [4]
[b] This present work
[c] Czocharalski method[2]

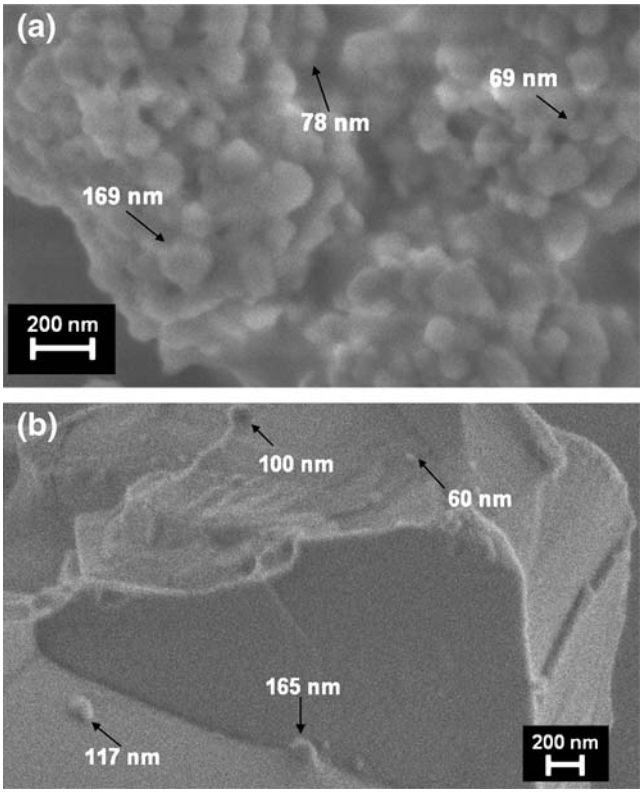

Fig. 4 HR-SEM micrograph of BEMO powders heat-treated at 700 °C (**a**) and 900 °C (**b**)

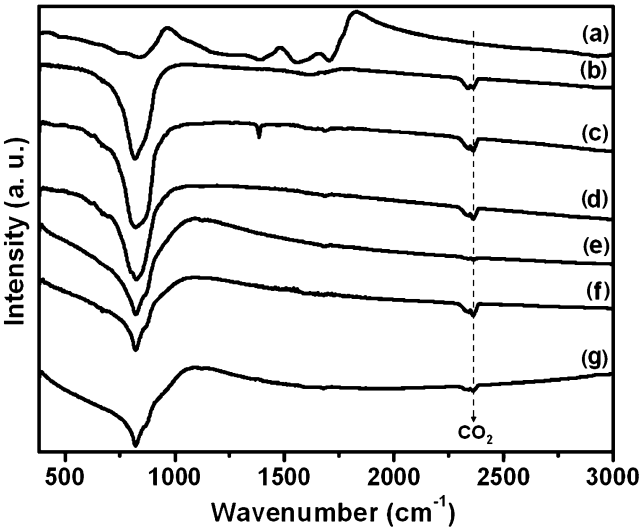

Fig. 5 FTIR absorption spectra of BEMO powders heat-treated at 350 °C (**a**), 400 °C (**b**), 500 °C (**c**), 600 °C (**d**), 700 °C (**e**), 800 °C (**f**) and 900 °C (**g**)

Figure 5 shows the FTIR spectra of the BEMO powders. Several bands ascribed to the carbonate groups are showed in the spectrum of BEMO annealed at 350 °C (Fig. 5a). According to Nakamoto, the υ(CO) stretching occurs at 2,375–1,100 cm^{-1} and the υ(OCO) stretching occurs at 1,100–550 cm^{-1}, showing that undecomposed organic ligands are still present in the powders [18]. The band at around 1,700 cm^{-1} is attributed to the vibration asymmetric COO. The bands of around 1,550 and 1,390 cm^{-1} are attributed to the vibration symmetric COO (Fig. 5a–c) [19]. The spectrum of Fig. 5d–g does not present any bands referent to carbonate groups. As it was presented previously in the Raman discussion, only the $F_2(\nu_3, \nu_4)$ (B_g and E_g) modes are IR active in the scheelite phase. The $F_2(\nu_3)$ vibrations are the antisymmetric stretches, and the $F_2(\nu_4)$ vibrations are bending modes. The spectra of the BEMO heat treated at 400–900 °C (Fig. 5b–g) display a very broad absorption band from 810 to 830 cm^{-1}, assigned to the $F_2(\nu_3)$ antisymmetric stretch vibrations, ascribed to the Mo–O stretching vibration in the MoO_4^{2-} tetrahedral [18]. The band at 2,350 cm^{-1} refers to the CO_2 adsorbed from the environment.

Figure 6 presents the room-temperature excitation spectrum of BEMO powder heat-treated at 700 °C obtained when the emission was fixed at 614 nm for illustration. In this spectrum it is noticed the characteristic excitation band of the Eu^{3+} $^5L_6$ transition at 394 nm as the main peak. The broad band at around 290 nm is ascribed to charge transfer from the matrix to the Eu^{3+} ion.

Figure 7 shows the room-temperature emission spectra of BEMO powders heat-treated at 500–900 °C. The study about the $CaMoO_4$:Eu^{3+} [5] deal with the variation of the relative intensity of same Eu^{3+} emissions related to the concentration of this ion, while the study made by us describe what is the behavior of the Eu^{3+} emission properties with the increase in the treated temperature in the $Ba_{0.99}Eu_{0.01}MoO_4$. BEMO powders presented the predominant red emission of the Eu^{3+} characteristic of its

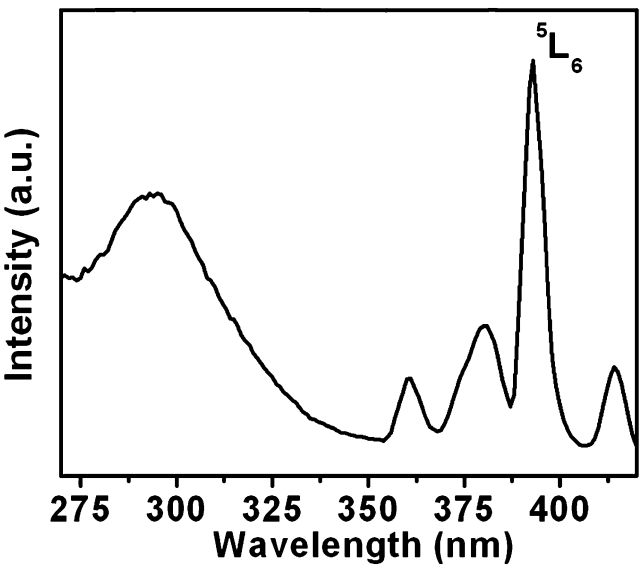

Fig. 6 Room-temperature excitation spectrum of BEMO powders heat-treated at 700 °C, $\lambda_{EM.}$=614 nm

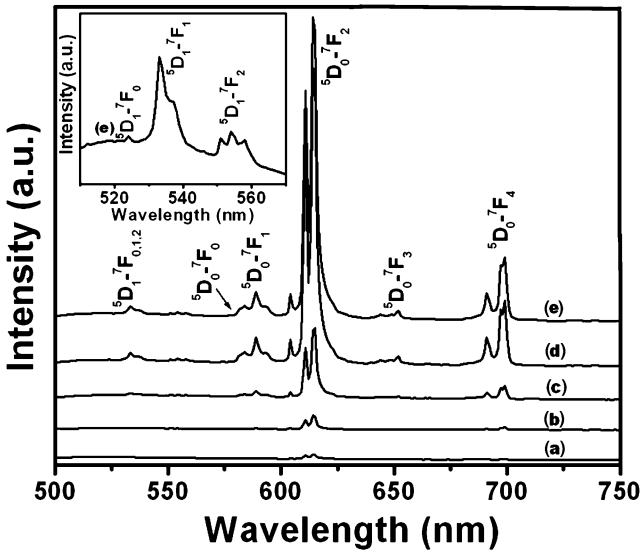

Fig. 7 Room-temperature emission spectra of the BEMO powders heat-treated at 500 °C (**a**), 600 °C (**b**), 700 °C (**c**), 800 °C (**d**) and 900 °C (**e**). $\lambda_{Exc.}$=394 nm

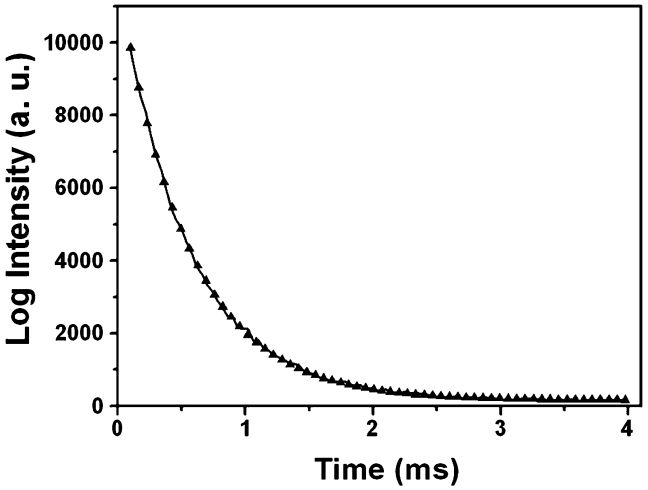

Fig. 8 Decay curve of the Eu^{3+} emission ($\lambda_{EM.}$=614 nm, $\lambda_{EXC.}$= 394 nm) for the BEMO powders heat-treated at 700 °C. Dotted line show the fit to first exponential function

$^5D_0 \rightarrow {}^7F_2$ emission when excited at 394 nm. The emission spectra of all samples presented the $^5D_1 \rightarrow {}^7F_0$, $^5D_1 \rightarrow {}^7F_1$ and $^5D_1 \rightarrow {}^7F_2$ transitions at 523, 533 and 554, respectively, besides the $^5D_0 \rightarrow {}^7F_0$, $^5D_0 \rightarrow {}^7F_1$, $^5D_0 \rightarrow {}^7F_2$, $^5D_0 \rightarrow {}^7F_3$ and $^5D_0 \rightarrow {}^7F_4$ Eu^{3+} ones at 578, 589, 614, 652 and 699 nm, respectively. This indicates that Eu^{3+} site symmetry has no center of inversion, so the state of opposite parity can be mixed in. In this system, the red lines will often be present and is predominant. The intensity of the $^5D_0 \rightarrow {}^7F_2$ transition, called as hypersensitive, is strongly dependent on the Eu^{3+} surrounding due to its electric dipole character. The $^5D_0 \rightarrow {}^7F_1$ transition however has a magnetic dipole character and its intensity is almost independent of the environment. So, the ratio of the $(^5D_0 \rightarrow {}^7F_2)/(^5D_0 \rightarrow {}^7F_1)$ emission intensity, gave us valuable information about the symmetry of the site in which Eu^{3+} ions are situated [20]. The emission spectra presented in Fig. 7 have the same profile where in all of them it is observed that the band ascribed to the $^5D_0 \rightarrow {}^7F_2$ transition at 614 nm is much more intense than that due to the $^5D_0 \rightarrow {}^7F_1$ at 589 nm. The emission spectra of the powders heat-treated at 800 and 900 °C showed a marked increase in its intensities compared to the materials heat-treated from 500 to 700 °C. It was also observed that the $(^5D_0 \rightarrow {}^7F_2)/(^5D_0 \rightarrow {}^7F_1)$ ratios increase with the increase of the heat treatment. This indicates a structural change of the Eu^{3+} to a lower symmetry.

Figure 8 shows the decay curve of the $^5D_0 \rightarrow {}^7F_2$ transition of the Eu^{3+} in the BEMO powder heat-treated at 700 °C, where the emission and excitation wavelengths were fixed at 614 nm and 394 nm, respectively, for illustration. Dotted line shows the fit to second exponential function. The decay times for the sample were evaluated and all of them presented the average value of 0.61 ms. Since the Eu^{3+} luminescence decay time follows one exponential curve and are similar for all samples it is supposed that only one type of Eu^{3+} center is present in the BEMO samples.

Conclusion

The Complex Polymerization Method (CPM) was used to prepare BEMO powders. The powders were annealed at 350, 400, 500, 600, 700, 800 and 900 °C for 2 h in a static atmosphere and with a heating rate of 5 °C/min. The BEMO materials show a crystalline $BaMoO_4$ scheelite-type phase after the heat treatment above up 400 °C. The lattice constants for the BEMO powders heat treated at 900 °C were a=5.5758(5) Å and c=12.794 (2) Å, while the pure BMO matrix presents a=5.5802 Å and c=12.821 Å. The ionic radius of Eu^{3+} (0.109 nm) is lower than the Ba^{2+} (0.149 nm) one; this difference resulted in lower lattice parameters for BEMO than the BMO matrix. This little difference in the lattice parameters indicates that Eu^{3+} is expected to occupy the Ba^{2+} site in this phosphor. The values of crystallite sizes (calculated using the (112), 100% diffraction peak) for the BEMO powders are near to 46 nm. These materials presented the characteristic red emission of the Eu^{3+} when excited at 394 nm. The emission spectra of the samples presented besides the $^5D_0 \rightarrow {}^7F_{1,\ 2,\ 3\ \text{and}\ 4}$ Eu^{3+} transitions at 589, 614, 652 and 699 nm, respectively, the $^5D_1 \rightarrow {}^7F_{0,\ 1\ \text{and}\ 2}$ at 523, 533, 554 nm, respectively. The emission spectra of the powders heat-treated at 800 and 900 °C showed a marked increase in its intensities compared to the materials heat-treated from 400 to 700 °C. Since the $^5D_0 \rightarrow {}^7F_2$ transition is much more intense than that due to the $^5D_0 \rightarrow {}^7F_1$ it is supposed that the symmetry

around the Eu^{3+} ions does not contain a center of inversion. It was also concluded that the surrounding around the Eu^{3+} have changed to a lower symmetry with the increase of temperature. The Eu^{3+} decay time was evaluated for all BEMO samples and all of them presented the average value of 0.61 ms. The mono exponential feature of the decay time curves indicates the presence of only one Eu^{3+} symmetry site.

Acknowledgements FAPERN, FAPESP-CEPID, CNPq and CAPES.

References

1. Ryu JH, Yoon JW, Lim CS, Oh WC, Shim KB (2005) Microwave-assisted synthesis of $CaMoO_4$ nano-powders by a citrate complex method and its photoluminescence property. J Alloys Compd 390(1–2):245–249
2. Cho WS, Yashima M, Kakihana M, Kudo A, Sakata T, Yoshimura M (1997) Active electrochemical dissolution of molybdenum and the application for room-temperature synthesis of crystallized luminescent calcium molybdate film. J Am Ceram Soc 80(3):765–769
3. Maurera MAMA, Souza AG, Soledade LEB, Pontes FM, Longo E, Leite ER, Varela JA (2004) Microstructural and optical characterization of $CaWO_4$ and $SrWO_4$ thin films prepared by a chemical solution method. Mater Lett 58:727–732
4. Marques APA, de Melo DMA, Paskocimas CA, Pizani PS, Joya MR, Leite ER, Longo E (2006) Photoluminescent $BaMoO_4$ nanopowders prepared by complex polymerization method (CPM). J Solid State Chem 179:658–665
5. Hu Y, Zhuang W, Ye H, Wang D, Zhang S, Huang X (2005) A novel red phosphor for white light emitting diodes. J Alloys Compd 390:226–229
6. Antipin AA, Katyshev AN, Kurkin IN, Shekun LY (1965) Paramagnetic resonance of erbium and europium in synthetic single crystals of $PbMoO_4$. Sov Phys, Solid State 7:1148
7. Kurkin IN, Tsvetkov EA (1970) Spin-lattice relaxation of Er^{3+} ions in a series of crystals homologous to scheelite. Sov Phys, Solid State 11:3027
8. Rosa ILV, Serra OA, Nassar EJ (1997) Luminescence study of the $[Eu(bpy)_2]^{3+}$ supported on Y zeolite. J Lumin 72–74:532–534
9. Barnes MD, Mehta A, Thundat T, Bhargava RN, Chabra V, Kulkarni B (2000) On–off blinking and multiple bright states of single europium ions in Eu^{3+}:Y_2O_3 nanocrystals. J Phys Chem B 104:6099–6102
10. Blasse G, Grabmaier BC (1994) Luminescent materials. Springer, Berlin
11. Blasse G, Bril A (1970) Characteristic luminescence. Philips Tech Rev 31(10):303
12. Ozuna O, Hirata GA, McKittrick J (2004) Luminescence enhancement in Eu^{3+}-doped α- and γ-Al_2O_3 produced by pressure-assisted low-temperature combustion synthesis. Appl Phys Lett 84(8):1296–1298
13. Bril A, Wanmaker WL (1966) New phosphors for colour television. Phillips Tech Rev 27:22
14. Serra OA, Zapparolli G, Nassar EJ, Rosa ILV (1995) A spectroscopic study of Eu^{3+}/hexamethylphosphoramide (HMPA) with hexafluorophosphate and perchlorate anions. J Braz Chem Soc 6(3):235–241
15. Richardson FS (1982) Terbium(III) and europium(III) ions as luminescent probes and stains for biomolecular systems. Chem Rev 82(5):541–552
16. Suryanarayana C, Norton MG (1998) X-ray diffraction: a practical approach. Plenum, New York
17. Basiev TT, Sobol AA, Voronko YuK, Zverev PG (2000) Spontaneous Raman spectroscopy of tungstate and molybdate crystal for Raman lasers. Opt Mater 15:205–216
18. Nakamoto K (1986) Infrared and Raman spectra of inorganic and coordination compounds, 4th edn. Wiley, New York
19. Pontes FM, Maurera MAMA, Souza AG, Longo E, Leite ER, Magnani R, Machado MAC, Pizani PS, Varela JA (2003) Preparation, structural and optical characterization of $BaWO_4$ and $PbWO_4$ thin films prepared by a chemical route. J Eur Ceram Soc 23:3001–3007
20. Rosa ILV, Maciel AP, Longo E, Leite ER, Varela JA (2006) Synthesis and photoluminescence study of $La_{1.8}Eu_{0.2}O_3$ coating on nanometric α–Al_2O_3. Mater Res Bull 41:1791–1797